Environmental Earth Sciences (2019) 78:388
https://doi.org/10.1007/s12665-019-8389-7

ORIGINAL ARTICLE

Analysis of dynamic compression property and energy dissipation of salt rock under three-dimensional pressure

Erbing Li[1] · Lei Gao[1,2] · Xiquan Jiang[3] · Jianli Duan[1] · Shiku Pu[1] · Jian Wang[1]

Received: 25 July 2018 / Accepted: 25 June 2019 / Published online: 3 July 2019

Abstract

In the study, a self-developed Split Hopkinson pressure bar apparatus with triaxial confining pressure was used to examine the dynamic compression property of salt rock under confining pressures of 5, 15, and 25 MPa. To examine the dynamic properties of salt rock, Yingcheng salt rock from Hubei province in China was considered. Dynamic stress–strain curves of salt rock under different confining pressures and strain rates were obtained. The results indicated that the peak stress and ductility of salt rock increased with increase in the strain rate although the strain rate strengthening effect of the salt rock was not evident with increase in the confining pressure. The dynamic properties and disintegration characteristics were investigated on the basis of the energy dissipation principle. The energy delivery and transformation in the entire experimental process were analyzed in detail. Under the same confining pressure, the hardening effect of the salt rock was more evident with increase in the incident energy, and this can be explained by the decrease in the energy transmission/absorption rate when the reflectance rate increased. Contrary to the plastic damage characteristics under quasi-static triaxial compression, the salt rock exhibited evident brittle fracture characteristics under dynamic compressive loading. The peak stress of the salt rock revealed different trends with the increase in energy absorption under different confining pressures. Increased energy absorption and higher peak stress were observed under low confining pressure. However, the peak stress significantly decreased with increase in the energy absorption under high confining pressure.

Keywords Salt rock · Split Hopkinson pressure bar (SHPB) · Energy dissipation · Three-dimensional pressure · Dynamic characteristics

Introduction

Oil and gas are stored in underground spaces created by water solution mining of deep salt deposits. This method is widely used in several countries including the United States, Germany, France, and Canada (Thoms and Gehle 2000). It is also an important measure of China's underground energy reserves (Zhang et al. 2017a). In contrast to the large thick salt domes formed by marine deposits in European and American countries, the salt rock in China exhibits a layered structure formed by lacustrine deposits. It exhibits three major characteristics including several layers of salt rock, a thin monolayer, and several insoluble interbeds (mainly including anhydrite layers, mudstone layers, and glauberite layers) (Liang et al. 2007; Meng et al. 2015; Liu et al. 2016a). The presence of the insoluble interbeds potentially causes the segmentation of the flow field during water solution mining, and leads to slow progress in building caverns. Additionally, the sudden collapse of an insoluble interbed may lead to engineering accidents such as the bending and smashing of the inner tubes installed in the injection well of the cavern and jamming of the casing, thereby severely affecting the progress in cavern building and even leading to an uncontrolled cavern shape (Meng et al. 2016; Zhang et al. 2017b). With respect to China's energy reserves in salt rock, the urgent issues that should be solved include efficiently controlling the insoluble interbed collapse, accelerating the

✉ Erbing Li
lebingest@126.com

✉ Lei Gao
gaolei@njust.edu.cn

[1] College of Defense Engineering, Army Engineering University of PLA, Nanjing 210007, Jiangsu, China

[2] College of Mechanical Engineering, Nanjing University of Science and Technology, Nanjing 210094, Jiangsu, China

[3] The No. 4 Department, Army Artillery and Air Defense Force College of PLA, Hefei 230031, Anhui, China

construction of water solution caverns, and building caverns with a larger volume. Currently, to obtain a controllable collapse of insoluble interbeds, the strategic reserve department of China's oil and gas is planning to adopt cumulative blasting technology to perform controlled blasting with respect to the thick insoluble interbeds. In this case, the surrounding rock of the salt cavern is in a three-dimensional dynamic mechanical state due to the impact of blasting and vibration waves due to blasting. Therefore, the dynamic characteristics of salt rock under three-dimensional pressure are extremely important and should be urgently investigated.

The dynamic characteristics of salt rock were recently analyzed (Mikhalyuk et al. 1998; Liu et al. 2012; Fang et al. 2012). The studies indicated that salt rock is sensitive to strain rate as mainly manifested by the strain-rate enhancement effect. However, the mechanical behavior and disintegration mechanism of salt rock under dynamic loads were not obtained. Specifically, energy characteristics are important indicators of the physical reaction and internal factors during the destruction of any material. Rock deformation and disintegration actually correspond to a process of energy dissipation and energy release (Zheng 1991; Bernabe and Revil 1995; Steffler et al. 2003; Sufian and Russell 2013; Wang et al. 2017). The dynamic deformation and disintegration characteristics of rocks, such as granite, sandstone, and coal gangue, are widely investigated using the energy dissipation principle (Jiang et al. 2005; Song et al. 2015; Deng et al. 2016; Liu et al. 2016b; Zhou et al. 2016). Tsouthrelis and Exadaktylos (1993) studied the effect of artificially created discontinuities in rock blocks on certain fracture energy parameters of Pendeli marble. Zhang et al. (2000) used a Split Hopkinson pressure bar (SHPB) testing system and a high-speed framing camera to quantitatively analyze the energy partitioning in the dynamic fracture process of a rock. Li et al. (2014) examined the effect of specimen size on the mechanical properties and energy dissipation characteristics of red sandstone using an SHPB system.

In the present study, salt rocks obtained from the Yingcheng deposit in Hubei Province, China were investigated. An independently developed SHPB test device that allows testing under confining pressure was utilized and dynamic compression tests of salt rocks were performed under three-dimensional pressures. The stress–strain curves of the salt rock under different confining pressures and strain rates were obtained. Based on the results obtained from the SHPB test on salt rock under three-dimensional pressure, the dynamic characteristics, energy dissipation, and disintegration mode of the salt rock under three-dimensional pressure were analyzed to provide references for the study on the dynamic properties of the salt rock and insoluble interbed blasting.

Salt rock samples and SHPB experimental device

Preparation of salt rock samples

The salt rock samples used in the tests mainly corresponded to gray white to white coarse glauberite salt rocks collected from the No. 4–15 salt bed of Yingcheng deposit in Hubei Province, China. The depth of the No. 4–15 salt bed approximately ranged from 600 to 800 m. The mineral composition of the salt rock was primarily NaCl with an average content of 70–80% with the lowest content at 65% and the highest content at 88.65%. The minor components were Na_2SO_4, $CaSO_4$, and water-insoluble materials with small amounts of $MgSO_4$ and $CaCO_3$, the contents of Na_2SO_4 and $CaSO_4$ were 4–6% and 7–16%, respectively, and the content of water-insoluble materials ranged from 2 to 13%.

With respect to nonuniform materials, such as coarse-grained rocks, performing the test using a larger diameter pressure bar system is considered more optimal (Dai et al. 2010). The tests were performed using a pressure bar system with a diameter of 75 mm. With an overall consideration for the effects of friction, inertia, and uniformity assumption, a slenderness ratio (the length to diameter ratio) of 0.5:1 is recommended for large specimens in SHPB tests (Zhou et al. 2012). Therefore, the salt rock samples were processed into cylindrical specimens of Φ 74 mm × 37 mm. The salt core was a cylinder with a diameter of 75–105 mm. Its required size was obtained through dry processes such as mechanical cutting and manual grinding. To prevent the specimens from causing corrosion due to a prolonged exposure to air (mainly due to moisture), the specimen surface was processed with varnish for waterproofing. Given the difficulty in salt rock coring and treating specimens and the presence of different impurities in the specimens, only 18 specimens with similar lithology, less impurity, and careful processing were selected for the test, and a set of six specimens were selected for each of the experiments under the confining pressures of 5, 15, and 25 MPa. The processed specimens are shown in Fig. 1, and the specimens and lithologic properties are listed in Table 1.

SHPB experimental device with confining pressure

An ordinary SHPB experimental device without confining pressure mainly consists of three parts: (1) a nitrogen cylinder that provides the initial velocity for the impact bar and dynamic system in a chamber. (2) The pressure bar system composed of a striker bar, an incident bar, and a transmission bar. (3) The data acquisition system is usually composed of a strain gage, a bridge box, a strain amplifier, an oscillometer, and a dynamic speed measuring instrument.

Fig. 1 Specimens of salt rock

Given the experimental difficulty under three-dimensional pressure, the SHPB experimental technology under confining pressure is immature and currently widely investigated (Nemat-Nasser et al. 2000; Rome et al. 2004; Bailly et al. 2011; Luo et al. 2011; Zhang and Zhao 2014). To perform the SHPB test on salt rock under three-dimensional pressure, a confining pressure device suitable for the SHPB test was designed, and the SHPB experimental device with confining pressure is shown in Fig. 2.

As shown in Fig. 2, the SHPB experimental device with confining pressure includes more parts than the ordinary SHPB experimental device as follows: (1) each of the two sides includes a pull bar, (2) a confining pressure device at the specimen, (3) a hydraulic cylinder at the end of the incident and transmission bars, (4) a single-action hydraulic cylinder, and (5) a large spring at the end of the incident bar. During the experiment, through an oil guide tube, the single-action hydraulic cylinder was connected with the hydraulic cylinder at the end of the incident and transmission bars to provide axial static pressure to the specimens. The single-action hydraulic cylinder was connected through an oil guide tube with the confining pressure device at the specimen to provide confining pressure to the specimens. Two long pull bars on both sides of the pressure bar were used as bars to bear the tension within the system due to the axial pressure. A butterfly spring (see Fig. 2b) with a large deformation capacity was added to the axial pressure device to better control the quality of the experiment, ensure the stability of the axial pressure applied during the experiment, and prevent the unloading of the axial pressure due to the deformation of the specimen during the impact.

The striker bar, incident bar, and transmission bar were composed of high-strength stainless steel with a density of 7850 kg/m^3 and an elastic modulus of 210 GPa. Their lengths were 300, 3500, and 2000 mm, respectively. The equipment for the test data acquisition system consisted of a KD7901 bridge box and KD6009 strain amplifier produced by Yangzhou Kedong Electronic Technology Institute in China and a DSO6014A oscillometer produced by Agilent, USA. Four sets of strain gages (see Fig. 3) were used in the experiment as follows: two groups of resistance strain gages (1$^{\#}$, 2$^{\#}$) on the incident bar, one set of resistance strain

Table 1 Characteristics of salt rock specimens

Specimen number	Thickness (mm)	Diameter (mm)	Weight (g)	Density (g/cm^3)	Lithology
1-1	34.78	73.88	323.95	2.173	Salt rock with a small admixture of glauberite
4-3	35.52	73.96	321.75	2.108	Salt rock with a small admixture of glauberite
222-2	34.78	73.72	316.93	2.135	Salt rock with a small admixture of glauberite
291-4	35.08	73.62	313.03	2.096	Salt rock with a small admixture of anhydrite
10-1	34.24	73.80	316.33	2.160	Salt rock with a small admixture of glauberite
222-3	36.02	73.90	326.43	2.113	Salt rock with a small admixture of glauberite
222-1	36.08	73.88	323.56	2.092	Salt rock with a small admixture of glauberite
3-4	34.36	73.78	307.47	2.093	Salt rock with a small admixture of glauberite
27	32.00	73.84	285.77	2.085	Salt rock with a small admixture of glauberite
291-6	36.08	73.70	338.29	2.198	Salt rock with a small admixture of anhydrite
222-4	35.96	73.82	323.20	2.100	Salt rock with a small admixture of glauberite
4-2	33.82	73.82	316.07	2.183	Salt rock with a small admixture of glauberite
291-1	36.08	73.70	338.29	2.198	Salt rock with a small admixture of glauberite
3-5	35.68	73.82	321.80	2.107	Salt rock with a small admixture of glauberite
291-3	35.22	73.96	323.13	2.136	Salt rock with a small admixture of glauberite
96-1	34.94	73.74	310.54	2.081	Salt rock with a small admixture of glauberite
291-2	35.80	73.76	333.39	2.180	Salt rock with a small admixture of glauberite
222-5	34.58	73.72	314.95	2.134	Salt rock with a small admixture of glauberite

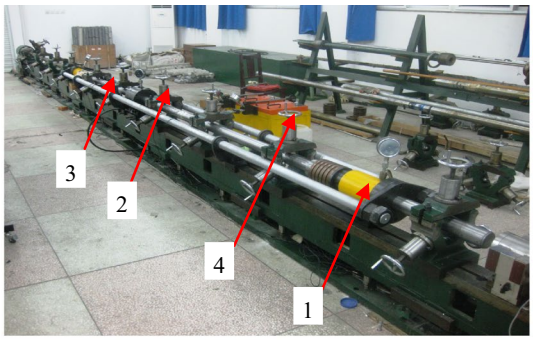

(a) Overall view

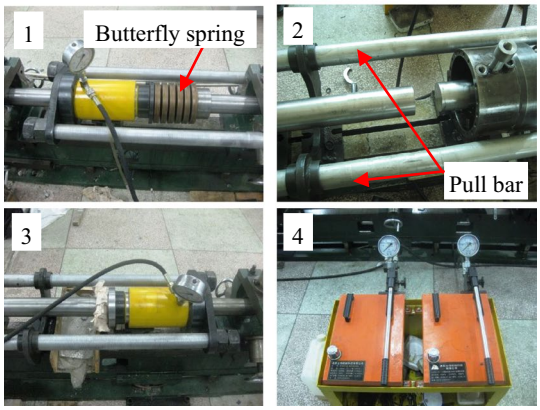

(b) Components

1—Hydraulic cylinder at the end of incident bar, 2—Circumferential confining pressure device
3—Hydraulic cylinder at the end of transmission bar, 4—Single acting hydraulic cylinder

Fig. 2 SHPB experimental device with the confining pressure system

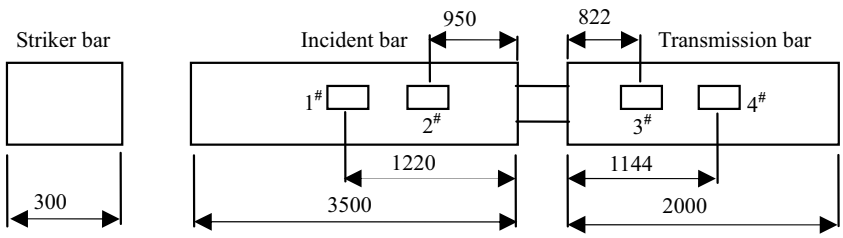

Fig. 3 Positions of strain gages $1^{\#}$ to $4^{\#}$ in the test (unit: mm)

gages ($4^{\#}$) and another set of higher sensitivity semiconductor strain gages ($3^{\#}$) on the transmission bar. Among them, strain gages $3^{\#}$ were mainly used to measure the transmission wave of stress information in the specimen.

Given the particularity of salt rock material, two technical measures were adopted for the experiment to ensure its validity and reliability. They are as follows: (1) the wave pattern shaping technique in which a piece of rubber sheet with a size of Φ 25 mm × 1 mm was pasted between the striker and incident bars to lengthen the incident wave rising edge, ensure the internal stress of the specimen is more uniform before its disintegration, and simultaneously eliminate the wave head overshoot and waveform oscillation of the stress pulse; (2) the use of a semiconductor strain gage with a sensitivity coefficient that is 58 times that of the resistance strain gage to measure the transmitted wave and to solve the problem of an unstable measurement of the weak signal of the transmitted wave resulting from the low wave impedance of the salt rock.

Analysis of energy composition during the SHPB test

Energy composition under static load

Prior to the dynamic test, a hydrostatic pressure was applied to the specimen, i.e., work was performed on the specimen,

and this component of the energy was recorded as U_0^e. After the dynamic test was completed, the axial pressure decreased, and the circumferential pressure increased due a few factors such as specimen deformation and static pressure state. Pressure relief involves releasing elastic strain energy, and this component of energy was recorded as U_1^e.

The work performed under hydrostatic pressure is obtained directly based on elastic mechanics and is given as follows:

$$U_0^e = \frac{\pi}{4} D^2 L \left[\frac{3}{2} \frac{(1-2\nu)}{E} \sigma_0^2 \right], \tag{1}$$

where D denotes the diameter of the specimen before the test, L denotes the length of the specimen before the test, σ_0 denotes the hydrostatic pressure, E denotes the elastic modulus under the σ_0 condition, and ν denotes the Poisson's ratio under the σ_0 condition.

The elastic strain energy that can be released was proposed by Xie et al. (2009) and is used as follows:

$$U_1^e = \frac{A_1 L_1}{2E_1} \left[\sigma_1^2 + 2\sigma_3^2 - 2\nu_1 \left(2\sigma_1\sigma_3 + \sigma_3^2 \right) \right], \tag{2}$$

where A_1 denotes the area of the specimen after the test, L_1 denotes the length of the specimen after the test, E_1 denotes the unloading elastic modulus (approximately the modulus in the elastic stage), ν_1 denotes the unloading Poisson's ratio (approximately the Poisson's ratio in the elastic stage), σ_1 denotes the axial pressure before unloading, and σ_3 denotes the circumferential confining pressure before unloading.

Energy composition under dynamic load

In the thermodynamic analysis of the SHPB test, the study object corresponded to the rock specimen and its static load device, while the other part corresponded to the environment except for the specimen. During the impact test, the energy loss caused by the friction between the specimen and bar was not considered. In the test system, based on the principle of energy conservation, the energy absorbed by the rock specimen and its static load device in the test process is expressed as follows (Lundberg 1976):

$$W_s(t) = W_I(t) - W_R(t) - W_T(t), \tag{3}$$

where $W_s(t)$ denotes the absorbed energy, $W_I(t)$ denotes the incident energy, $W_R(t)$ denotes the reflected energy, and $W_T(t)$ denotes the transmitted energy.

According to the basic assumption for the SHPB test, the stress wave in the test bar was considered as a one-dimensional elastic wave. Based on 1D elastic wave theory, the formula for calculating the energy of the incident wave, reflected wave, and transmitted wave is as follows (Lundberg 1976):

$$W_x(t) = \frac{AC_0}{E_0} \int_0^t \sigma_x^2(t)\mathrm{d}t, \tag{4}$$

where x represents I, R, and T that correspond to the incident wave, reflected wave, and transmitted wave, respectively; A denotes the area of the bar; C_0 denotes the stress wave velocity in the bar; E_0 denotes the elastic modulus of the bar; and $\sigma_I(t)$, $\sigma_R(t)$, and $\sigma_T(t)$ denote the time history of the incident, reflected, and transmitted stress, respectively.

In the elastic stage, the stress wave velocity is expressed by the mass density and elastic modulus of the compression bar as follows:

$$C_0 = \sqrt{\frac{E_0}{\rho_0}}, \tag{5}$$

where ρ_0 denotes the mass density of the bar.

Thus, the energy formula of the stress wave is simplified as follows:

$$\begin{cases} W_I(t) = \frac{A}{C_0\rho_0} \int_0^t \sigma_I^2(t)\mathrm{d}t \\ W_R(t) = \frac{A}{C_0\rho_0} \int_0^t \sigma_R^2(t)\mathrm{d}t \\ W_T(t) = \frac{A}{C_0\rho_0} \int_0^t \sigma_T^2(t)\mathrm{d}t. \end{cases} \tag{6}$$

During the dynamic test, the specimens suffered impact disintegrations. However, the debris produced by the disintegration of specimens was limited by the three-directional static pressure. Therefore, the kinetic energy of debris was not considered. The specimens were considered as the object of study. Based on the conservation of energy, the formula is obtained as follows:

$$W_s(t) + U_0^e = U_d + U_1^e, \tag{7}$$

where U_d denotes the energy consumed by the disintegration of the specimen to a certain extent of damage (the energy consumed by the plastic deformation of the specimen, energy consumed by the negative work of confining pressure, and energy consumed by the newly created surface area and cracks). Given that U_0^e and U_1^e are low relative to the dynamic energy, the two values offset each other based on Eq. (7). Thus, this part of the energy was ignored in the analysis.

Salt rock SHPB tests and analysis of results

Test method and procedure

The rock specimen was first placed in a Hopkinson pressure bar system equipped with the confining pressure device and the axial and circumferential static pressures were then applied through the additional hydraulic cylinder for the

specimen. After the three-dimensional pressure requirement was satisfied, an axial impact on the specimen was performed until its disintegration, and the signals and data were then recorded by the data acquisition system. The main steps of the test include specimen preparation, adjustment of the pressure bar system, erection of the confining pressure device, installation of strain gages, impact test without the specimen in place, impact test by applying axial pressure and without the specimen in place, impact test by applying three-dimensional pressure, acquisition and analysis of the waveform signals, and analysis and processing of data after the test.

Prior to the impact–compression test on the salt rock under three-dimensional pressure, the propagation velocity of the wave in the pressure bar and the strain–voltage conversion coefficients in all channels were calibrated using the impact test without the specimen in place. The results indicated that the strain–voltage conversion coefficients of channels 1, 2, 3, and 4 were 2518.89 εμ/v, 2596.80 εμ/v, 116.23 εμ/v, and 2518.89 εμ/v, respectively. The propagation velocity of the wave in the pressure bar was 5160 m/s. When the SHPB test was performed on the salt rock under three-dimensional pressure, the impact velocity of the striker bar was adjusted by changing the output pressure of the nitrogen gas cylinder, thereby achieving a variable strain rate loading. The typical waveforms of the strain gages under different confining pressure are shown in Fig. 4, and the σ_c in the figure denotes the confining pressure. As shown in Fig. 4, the waveform signals are normal. This indicated that the design and debugging of the test device was reasonable, and thus the SHPB tests under confining pressure were performed.

The results obtained in the test corresponded to the waveforms displayed on the oscillometer. Based on the waveforms, the stress and strain of the salt specimens were calculated. In the test, channels 1 and 2 were used to record the incident and reflected waves via the electrical resistance strain gages with a sensitivity coefficient of 2. Channels 3 and 4 were used to record the transmitted wave. Given the material characteristics of the salt rock, a semiconductor strain gage with a sensitivity coefficient of 116 was adopted in channel 3 while an electrical resistance strain gage with a sensitivity coefficient of 2 was adopted in channel 4.

Test results and analysis

Based on 1D stress wave theory (Kolsky 1964), the strain rate of the specimen is determined through the three-wave method, and exhibits the following form (Frew et al. 2001; Wang and Shang 2014):

$$\dot{\varepsilon}(t) = \frac{c_0}{l_s}(\varepsilon_I - \varepsilon_R - \varepsilon_T), \tag{8}$$

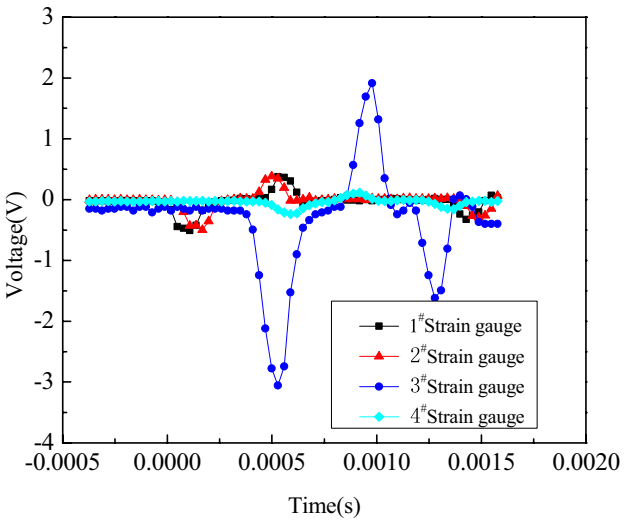

(a) σ_c =5 MPa (specimen 222-3)

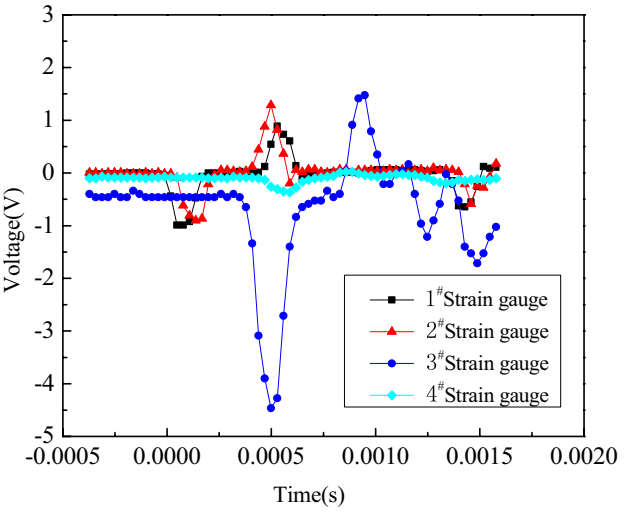

(b) σ_c =15 MPa (specimen 27)

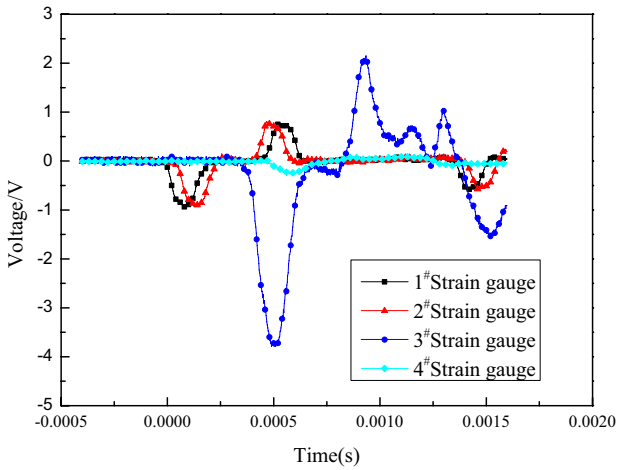

(c) σ_c =25 MPa (specimen 291-3)

Fig. 4 Typical waveforms measured by strain gages under different confining pressures

where $\dot{\varepsilon}(t)$ denotes the strain rate history of the tested specimen, c_0 denotes the elastic wave velocity in the bar material, l_s denotes the length of the specimen; ε_I, ε_R, and ε_T denote the incident, reflected, and transmitted strain histories, respectively.

The strain waves of the incident wave, reflected wave, and transmitted wave were calculated based on the conversion coefficients calibrated before the tests. Using the aforementioned Eqs. (1)–(8), the energy values for each part of the test were obtained, and the calculated results are shown in Table 2.

Figure 5 shows the effect of confining pressure on the stress–strain curve for three types of average strain rates. In the figure, $\dot{\varepsilon}$ denotes the strain rate of the tested specimen, and $\bar{\dot{\varepsilon}}$ denotes the average strain rate. As shown in Fig. 5, under a similar strain rate, when a confining pressure was applied on the salt rock, the effect on the mechanical behavior of the salt rock was not evident.

Figure 6 shows the uniaxial compression curves of the salt rock under different strain rates (Liu et al. 2012). An increase in strain rate significantly affected the strength enhancement of the salt rock without confining pressure although the peak strain essentially remained unchanged. Figure 7 shows the dynamic stress–strain curves of the salt rock under different confining pressures. The experimental data indicated that under the same confining pressure and a variable strain rate, the salt rock under confining pressure continued to correspond to a rate-sensitive material. The peak strength and ductility of salt rock increase with increases in the strain rate although the strengthening effect of the strain rate under high confining pressures (15 MPa and 25 MPa) was less significant than that under a low confining pressure (5 MPa) and uniaxial compression (see Fig. 6). This was because the coarse-grained rock was similar to the concrete material in the SHPB experiment, and its compressive strength varied with strain rate mainly due to the confining pressure caused by inertia, and thus it did not really correspond to a strain rate effect (Zhang et al. 2009). However, the inertia effect under high confining pressure was no longer evident, and the converted strain rate was not evident. Therefore, the strain rate strengthening effect of the salt rock under high confining pressure was evidently lower than that in low confining pressure or no confining pressure.

Energy dissipation law during the disintegration of salt rocks

Energy distribution law in the SHPB test

In the SHPB test system, the incident energy is the main source of energy, and its value depends on the impact velocity of the striker bar (or the air pressure controlling the striker bar velocity). In comparison, the reflected energy, transmitted energy, and absorbed energy of the rock mainly depends on the nature of the rock itself and on the wave impedance difference between the rock and test bar. Therefore, the ratio of the reflected energy, transmitted energy, and

Table 2 Calculation of results with respect to energy

Specimen number	Confining pressure (MPa)	Strain rate (s^{-1})	Peak stress (MPa)	W_I (J)	W_R (J)	W_T (J)	W_s (J)
1-1	5	140	112.30	328.3	180.4	53.3	94.5
222-3	5	240	111.20	754.4	425.4	151.7	177.6
4-3	5	426	149.09	1967.0	1272.0	252.6	442.3
222-2	5	519	158.28	2474.5	1668.7	296.8	509.0
291-4	5	650	193.73	3434.4	2987.8	275.8	170.8
10-1	5	695	167.86	3466.7	2584.8	418.8	463.1
222-1	15	440	168.96	2020.7	1353.4	255.8	411.6
3-4	15	476	158.73	1892.1	1313.7	261.7	316.7
291-6	15	508	190.99	2906.9	2049.0	354.3	503.7
4-2	15	535	163.21	3018.4	2274.8	321.0	422.6
27	15	550	165.16	2808.4	1907.6	290.3	610.6
222-4	15	631	175.96	3548.3	2404.0	321.5	822.8
291-1	25	430	163.41	2162.2	1023.2	306.7	832.3
3-5	25	433	142.45	2088.3	1029.3	218.4	840.6
291-3	25	513	155.58	2629.1	1512.7	274	841.8
96-1	25	560	140.77	2839.3	1821.0	194.2	824.2
291-2	25	574	155.28	3445.1	1920.2	262.1	1262.8
222-5	25	597	186.25	1845.3	871.5	293.8	680.1

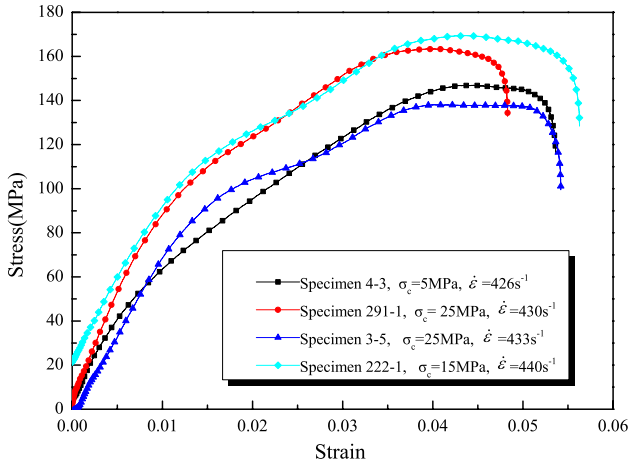

(a) $\bar{\dot{\varepsilon}}$ =430 s^{-1}

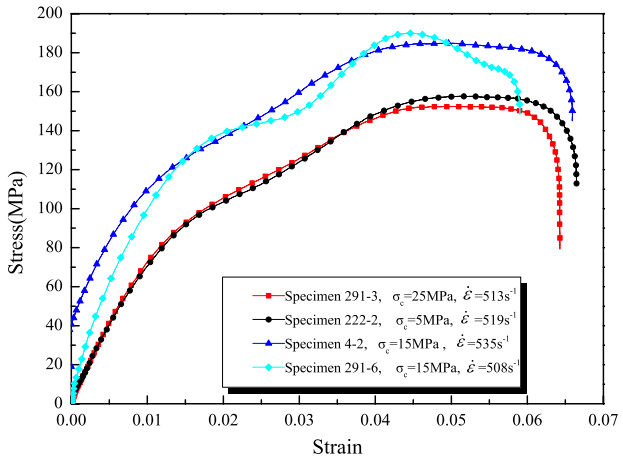

(b) $\bar{\dot{\varepsilon}}$ =520 s^{-1}

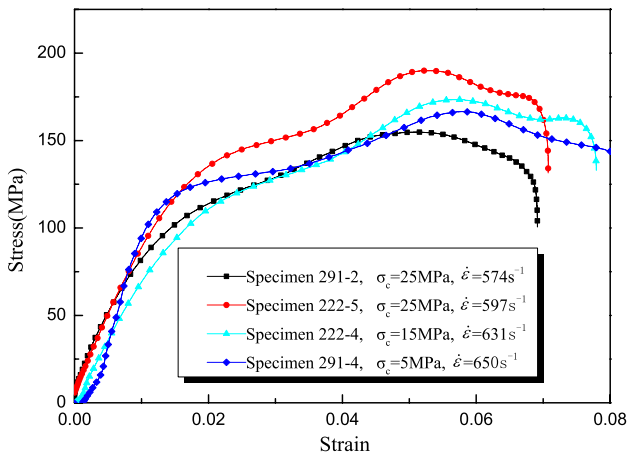

(c) $\bar{\dot{\varepsilon}}$ =610 s^{-1}

Fig. 5 Effect of confining pressure on stress–strain curves under high strain rates

absorbed energy to the incident energy is used, namely, the energy's reflectivity, transmissivity, and absorptivity better

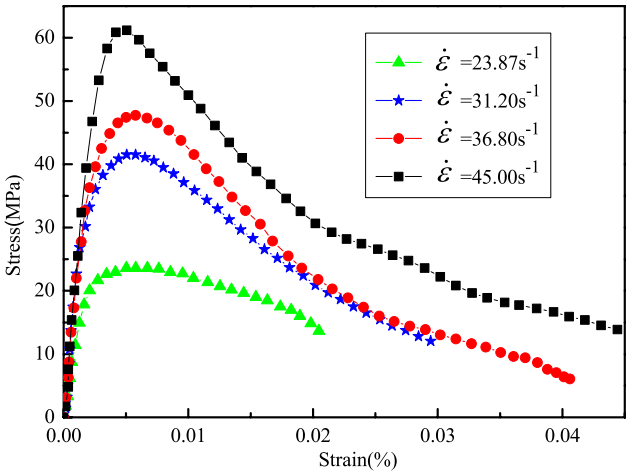

Fig. 6 Stress–strain curves of salt rock under uniaxial compression and different strain rates (Liu et al. 2012)

reflect the dynamic response of the test specimens to the stress wave.

Figure 8 shows the relationship curves between the reflectivity, transmissivity, and absorptivity of energy and the incident energy of the salt rock under different confining pressures as obtained from Table 2. As shown in Fig. 8, under different confining pressures, the distribution ratio of energy exhibits the same variation trend with increases in the incident energy. The energy transmissivity and absorptivity decrease with increases in the incident energy while the energy reflectivity increases with increases in the incident energy. The variation trend indicates that most of the energy is reflected back with increases in the incident energy.

Effect of confining pressure on energy distribution

Figure 9 shows the relationships between three types of energy distribution ratios and confining pressures. To reduce the effects of incident energy and other factors on the analysis of the confining pressure, the data with similar incident energy are adopted in the diagram. As shown in Fig. 9, increases in the confining pressure decrease the energy reflectivity and transmissivity while the energy absorptivity increases. The phenomenon is evidently different from the corresponding pattern of sandstone. Based on several tests, Lv et al. (2011) concluded that under the impact load, the energy absorptivity of sandstone decreases with increases in the confining pressure.

The reason for the difference in the characteristics of sandstone is that the crack growth in sandstone in the tests significantly reduces with increases in the confining pressure. Therefore, under the same incident energy, increases in the confining pressure increase the difficulty of developing cracks, and less energy is consumed. However, increases in

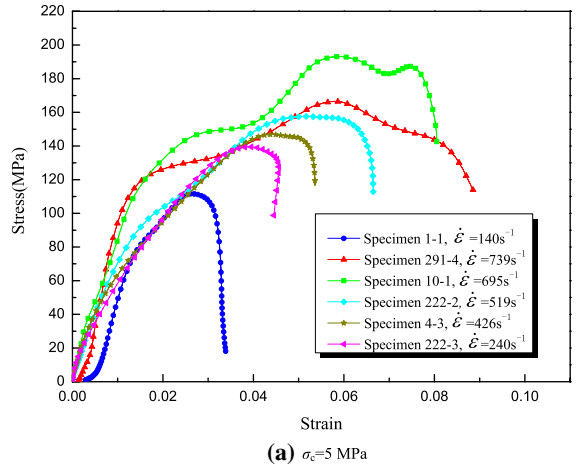

(a) σ_c=5 MPa

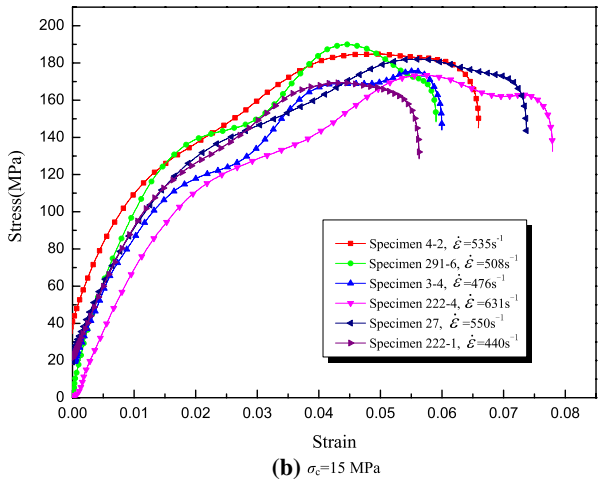

(b) σ_c=15 MPa

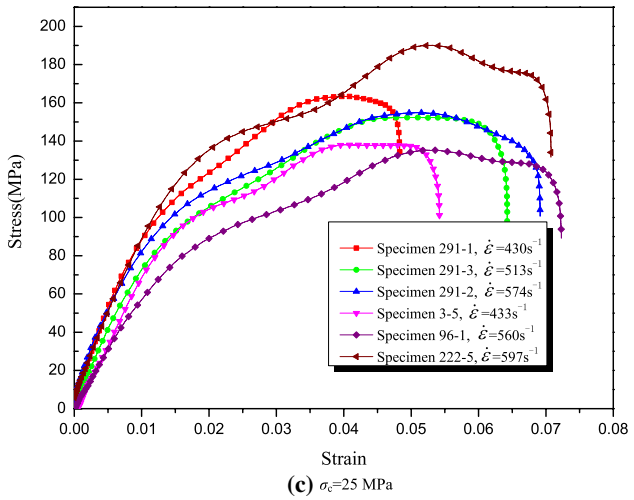

(c) σ_c=25 MPa

Fig. 7 Stress–strain curves of the salt rock under high strain rates and confining pressure

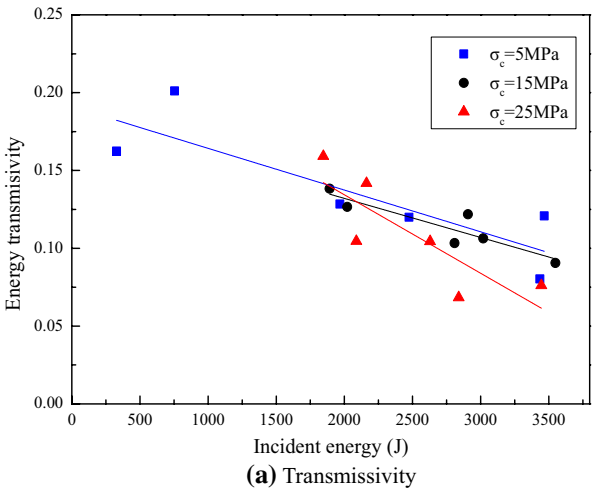

(a) Transmissivity

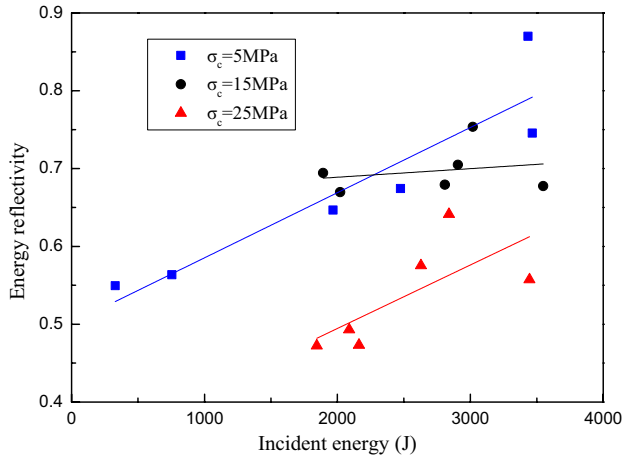

(b) Reflectivity

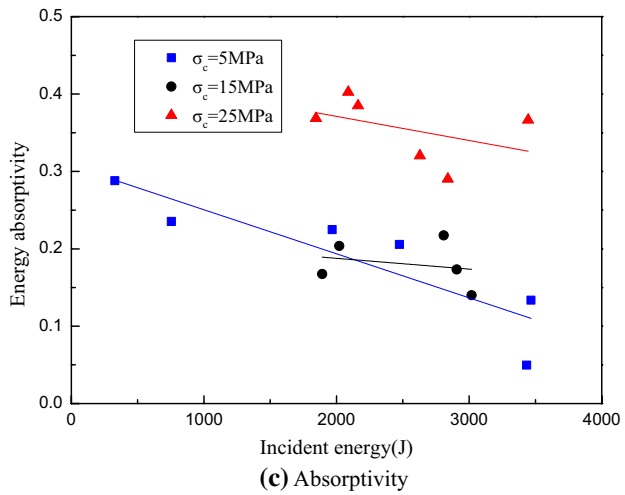

(c) Absorptivity

Fig. 8 Relationship between the energy distribution ratio and incident energy

the confining pressure make the plastic flow properties of salt rock stronger and increase the energy that is absorbed and consumed. When compared to the sandstone, the confining pressure improves the plastic deformation capacity of the salt rock and thereby enhances the effect of absorbing energy.

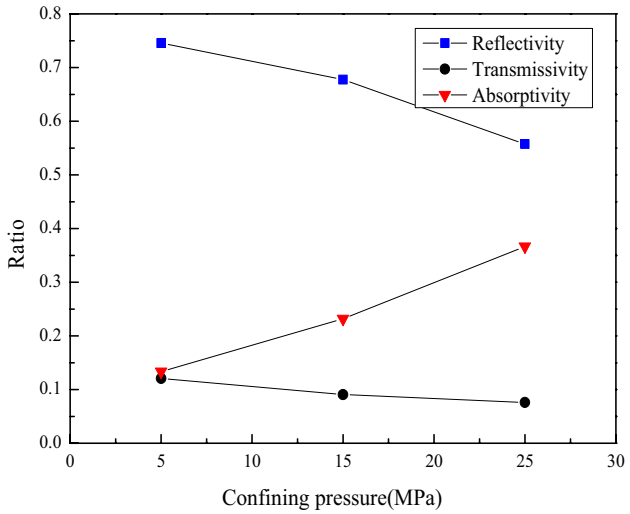

Fig. 9 Relationships between energy reflectivity, transmissivity, absorptivity, and confining pressure

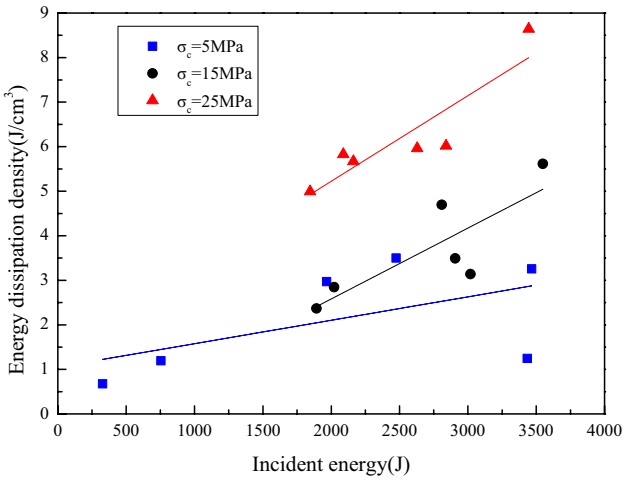

Fig. 10 Relationship between energy dissipation density and incident energy under different confining pressures

As shown in Fig. 10, the energy density increases with increases in the incident energy. Increases in the incident energy increase the energy distributed to each part and increase the energy density. As shown in the figure, the energy density under the confining pressure of 25 MPa significantly exceeds that under the confining pressure of 5 MPa. Furthermore, with increases in the incident energy, the confining pressure increases and the energy density rapidly increases. The change in the pattern is analyzed in Fig. 9. Under similar incident energy, increases in the confining pressure increase the energy absorbed, thereby significantly increasing the energy density.

Relationship between energy absorption and peak stress

To avoid the effect of the time factor, the concept of an average energy absorption power is introduced as follows:

$$P = \frac{W_s}{t}, \tag{9}$$

where W_s denotes the absorbed energy, and t denotes the impact time.

Figure 11 shows the relationship between the average energy absorption power and the peak stress of the specimen. As shown in Fig. 11, under different confining pressures, the salt rock peak stress exhibits different changing trends with the average energy absorption power. Specifically, under 25 MPa of confining pressure, the salt rock peak stress decreases with increases in the average energy absorption power.

Under a high confining pressure, a stronger flow plasticity of salt rock represents the characteristics of soft material, i.e., the stress wave propagation in soft material is uneven and results in disproportion among the strain rate and reflected wave and between the stress and transmitted wave (Chen et al. 2002). During the impact, with increases in the plastic deformation and hardening, the salt rock also represents the characteristics of a brittle material, and thus the peak stress is not positively correlated with incident energy and average energy absorption power.

Influence of energy absorption on disintegration characteristics

Under the quasi-static condition, the salt rock is a typical soft rock and typically exhibits tensile disintegration characteristics along the axial direction under uniaxial compression

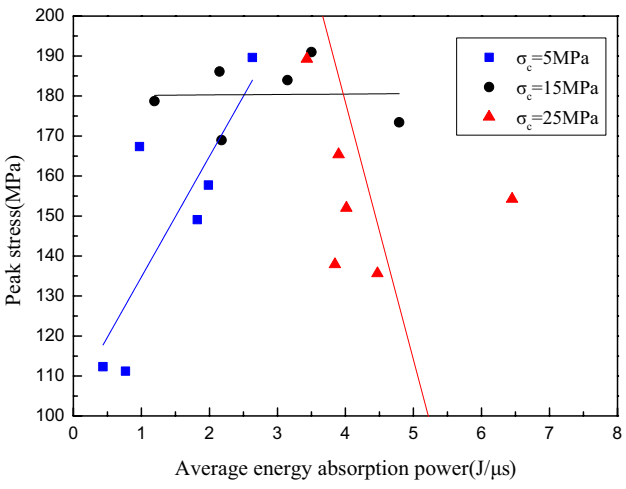

Fig. 11 Relationship between average power of absorbed energy and peak stress under different confining pressures

although it exhibits an evident elastic–plastic deformation behavior under triaxial compression (Yang et al. 1999; Liang et al. 2007; Ma et al. 2013). When the confining pressure exceeds 5 MPa, the salt rock even exhibits excellent ductility and "no disintegration" characteristics. Conversely, under dynamic loading, brittle fracture occurs even when the confining pressure increases (as shown in Fig. 12).

The mechanism of the phenomenon is explained from the angle of energy analysis. Under the same confining pressure, when the salt rock specimen exhibits less energy absorption, the energy absorbed by the specimen is only used for plastic deformation and hardening. When the energy absorbed by the specimen increases, the plastic deformation does not completely consume the absorbed energy, and excess energy is subsequently dissipated through other methods such as microcracks and friction heat generation. When the absorbed energy is significantly high, such as under dynamic loading, the absorbed energy exceeds the consumed energy for plastic deformation, strain hardening, and microcracks, and the excess energy makes the specimen produce new surface area. Increases in the residual energy increase the surface area and the specimen appears as more crushing.

As shown in Fig. 12, when the incident energy is the same or similar, with increase in the confining pressure, the larger the fragments after the specimen was destroyed. This is because increase in the confining pressure increases the energy consumed by the plastic deformation of salt rock, makes the dislocation of crystal in salt rock more significant, increases the energy for expanding crack, and generates a new surface area. Thus, with respect to the same or similar incident energy, when the confining pressure is low, the fragments of salt rock are smaller although there are several salt rock crystals (smaller dislocation of crystal). Conversely, when the confining pressure is high, the fragments of salt rock are larger although there are several microcracks in the fragments (larger dislocation of crystal).

Conclusions

In the study, an independently developed experimental device was used to perform dynamic compression tests on salt rocks obtained from the Yingcheng deposit, China, under three-dimensional pressure at confining pressures of 5 MPa, 15 MPa, and 25 MPa. The stress–strain curves of the salt rock under three-dimensional pressure were obtained. The test results indicated that the salt rock under dynamic load is a type of rate-dependent material, and the peak stress and ductility of salt rock increase with increases in the strain rate, although the strain rate strengthening effect of the salt rock under high confining pressure is evidently lower than that under a low or zero confining pressure.

The energy absorption efficiency of the salt rock was directly related to the input energy and confining pressure. Under the same confining pressure during the impact, the salt rock developed plastic deformation accompanied by hardening. Increases in the incident energy accelerated the hardening rate of the salt rock and decreased the absorptivity and transmissivity of energy while increasing the reflectivity of energy. Under the same or similar energy input, increases in the confining pressure increased the flow plasticity of the salt rock and the absorptivity of energy while decreasing the transmissivity and reflectivity of energy.

Under dynamic compressive loading, the rock salt exhibited evident brittle fracture characteristics. The peak stress of the salt rock under different confining pressures indicated a different variation pattern with respect to the average energy-absorbing power. Under a low confining pressure ($\leq$ 15 MPa), the peak stress increased with increases in the average energy-absorbing power and decreased with increases in the confining pressure. At a higher confining pressure (25 MPa), the peak stress decreased with increases in the average energy-absorbing power, thereby indicating that the confining pressure changed the internal energy distribution ratio of the specimen.

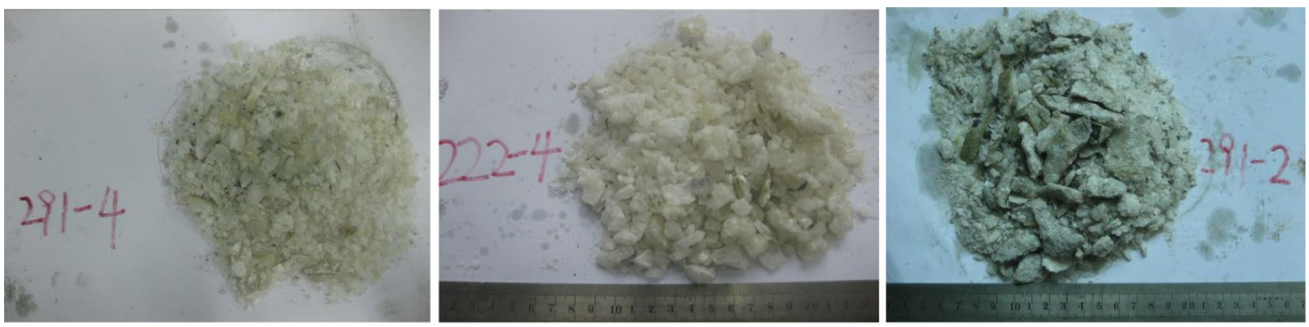

(a) σ_c=5 MPa, W_I =3434.4 J **(b)** σ_c=15 MPa, W_I = 3548.3 J **(c)** σ_c=25 MPa, W_I = 3445.1 J

Fig. 12 Images of failure under different confining pressures albeit approximately equal incident energy

Acknowledgements The study is fully sponsored by the National Natural Science Foundation for Young Scientists of China (Grant no. 51408605), and the authors gratefully acknowledge the same. The authors wish to thank Prof. J.J.K. Daemen at the University of Nevada, USA for his suggestions and help.

References

Bailly P, Delvare F, Vial J, Hanus JL, Biessy M, Picart D (2011) Dynamic behavior of an aggregate material at simultaneous high pressure and strain rate: SHPB triaxial tests. Int J Impact Eng 38:73–84. https://doi.org/10.1016/j.ijimpeng.2010.10.005

Bernabe Y, Revil A (1995) Pore-scale heterogeneity, energy dissipation and the transport properties of rocks. Geophys Res Lett 22(12):1529–1532. https://doi.org/10.1016/0148-9062(96)85059-5

Chen W, Lu F, Frew DJ, Forrestal MJ (2002) Dynamic compression testing of soft materials. J Appl Mech 69(3):214–223. https://doi.org/10.1115/1.1464871

Dai F, Huang S, Xia K, Tan Z (2010) Some fundamental issues in dynamic compression and tension tests of rocks using split Hopkinson pressure bar. Rock Mech Rock Eng 43:657–666. https://doi.org/10.1007/s00603-010-0091-8

DengY Chen M, Jin Y, Zou DW (2016) Theoretical analysis and experimental research on the energy dissipation of rock crushing based on fractal theory. J Nat Gas Sci Eng 33:231–239. https://doi.org/10.1016/j.jngse.2016.05.020

Fang Q, Ruan Z, Zhai CC, Jiang XQ, Chen L, Fang WM (2012) Split Hopkinson pressure bar test and numerical analysis of salt rock under confining pressure and temperature. Chin J Rock Mech Eng 31(9):1756–1765. http://www.rockmech.org/CN/Y2012/V31/I9/1756

Frew DJ, Forrestal MJ, Chen W (2001) A split Hopkinson pressure bar technique to determine compressive stress-strain data for rock materials. Exp Mech 41(1):40–46. https://doi.org/10.1007/BF02323102

Jiang Y, Zang SX, Wei RQ (2005) Decibel error test and flow law of multiphase rocks based on energy dissipation theory. Earth Planet Sci Lett 235:200–210. https://doi.org/10.1016/j.epsl.2005.03.014

Kolsky H (1964) Stress waves in solids. J Sound Vib 1(1):88–110. https://doi.org/10.1016/0022-460X(64)90008-2

Li M, Mao XB, Lu AH, Tao J, Zhang GH, Zhang LY, Li C (2014) Effect of specimen size on energy dissipation characteristics of red sandstone under high strain rate. Int J Min Sci Technol 24:151–156. https://doi.org/10.1016/j.ijmst.2014.01.002

Liang WG, Yang CH, Zhao YS, Dusseault MB, Liu J (2007) Experimental investigation of mechanical properties of bedded salt rock. Int J Rock Mech Min Sci 44:400–411. https://doi.org/10.1016/j.ijrmms.2006.09.007

Liu WG, Wang XJ, Jiang XQ (2012) Study of the dynamic behavior and constitutive relation of salt rock acted by impact loading. J Exp Mech 27(3):295–300 **(in Chinese)**

Liu W, Muhammad N, Chen J, Spiers CJ, Peach CJ, Jiang DY, Li YP (2016a) Investigation on the permeability characteristics of bedded salt rocks and the tightness of natural gas caverns in such formations. J Nat Gas Sci Eng 35:468–482. https://doi.org/10.1016/j.jngse.2016.07.072

Liu XS, Ning JG, Tan YL, Gu QH (2016b) Damage constitutive model based on energy dissipation for intact rock subjected to cyclic loading. Int J Rock Mech Min Sci 85:27–32. https://doi.org/10.1016/j.ijrmms.2016.03.003

Lundberg B (1976) A split Hopkinson bar study of energy absorption in dynamic rock fragmentation. Int J Rock Mech Min Sci Geomech Abstr 13(6):187–197. https://doi.org/10.1016/0148-9062(76)91285-7

Luo H, Lu H, Cooper WL, Komanduri R (2011) Effect of mass density on the compressive behavior of dry sand under confinement at high strain rates. Exp Mech 51(9):1499–1510. https://doi.org/10.1007/s11340-011-9475-2

Lv XC, Xu JY, Zhao DH, Ge HH, Wang ZD (2011) Research on confining pressure effect of sandstone dynamic mechanical performance under the cyclical impact loadings. Eng Mech 28(1):138–144 **(in Chinese)**

Ma LJ, Liu XY, Wang MY, Xu HF, Hua RP, Fan PX, Jiang SR, Wang GA, Yi QK (2013) Experimental investigation of the mechanical properties of rock salt under triaxial cyclic loading. Int J Rock Mech Min Sci 62:34–41. https://doi.org/10.1016/j.ijrmms.2013.04.003

Meng T, Hu YQ, Fang RL, Kok J, Fu QN, Feng G (2015) Study of fracture toughness and weakening mechanisms in gypsum interlayers in corrosive environments. J Nat Gas Sci Eng 26:356–366. https://doi.org/10.1016/j.jngse.2015.06.027

Meng T, Hu YQ, Fang RL, Fu QN, Yu WD (2016) Weakening mechanisms of gypsum interlayers from Yunying salt cavern subjected to a coupled thermo-hydro-chemical environment. J Nat Gas Sci Eng 27:77–89. https://doi.org/10.1016/j.jngse.2016.01.039

Mikhalyuk AV, Zakharov VV, Parshukov PA (1998) Rock salt under nonequilibrium dynamic loads. J Min Sci 34(1):1–9. https://doi.org/10.1007/BF02765518

Nemat-Nasser S, Isaacs J, Rome J (2000) Triaxial Hopkinson techniques. ASM handbook, mechanical testing and evaluation. ASM Int Mater Park OH 8:516–518

Rome J, Isaacs J, Nemat-Nasser S (2004) Hopkinson techniques for dynamic triaxial compression tests. In: Gdoutos E (ed) Recent advances in experimental mechanics. Springer, Amsterdam, pp 3–12. https://doi.org/10.1007/0-306-48410-2_1

Song DZ, Wang EY, Li ZH, Liu J, Xu WQ (2015) Energy dissipation of coal and rock during damage and failure process based on EMR. Int J Min Sci Technol 25:787–795. https://doi.org/10.1016/j.ijmst.2015.07.014

Steffler ED, Epstein JS, Conley EG (2003) Energy partitioning for a crack under remote shear and compression. Int J Fract 120(4):563–580. https://doi.org/10.1023/A:1025511703698

Sufian A, Russell AR (2013) Microstructural pore changes and energy dissipation in Gosford sandstone during pre-failure loading using X-ray CT. Int J Rock Mech Min Sci 57:119–131. https://doi.org/10.1016/j.ijrmms.2012.07.021

Thoms RL, Gehle RM (2000) A Brief history of salt cavern use. In: Geertman RM (ed) Proceedings of 8th world salt symposium, vol 1. Elsevier, Amsterdam, pp 207–214

Tsouthrelis CE, Exadaktylos GE (1993) Effect of rock discontinuities on certain rock strength and fracture energy parameters under uniaxial compression. Geotech Geol Eng 11(2):81–105. https://doi.org/10.1016/0148-9062(94)92412-0

Wang TT, Shang B (2014) Three-wave mutual-checking method for data processing of SHPB experiments of concrete. J Mech 30(5):5–10. https://doi.org/10.1017/jmech.2014.55

Wang P, Xu JY, Fang XY, Wang PX (2017) Energy dissipation and damage evolution analyses for the dynamic compression failure process of red-sandstone after freeze–thaw cycles. Eng Geol 221:104–113. https://doi.org/10.1016/j.enggeo.2017.02.025

Xie HP, Li LY, Peng RD, Ju Y (2009) Energy analysis and criteria for structural failure of rocks. J Rock Mech Geotech Eng 1(1):11–20. https://doi.org/10.3724/sp.j.1235.2009.00011

Yang CH, Daemen JJK, Yin JH (1999) Experimental investigation of creep behavior of salt rock. Int J Rock Mech Min Sci 36:233–242. https://doi.org/10.1016/S0148-9062(98)00187-9

Zhang QB, Zhao J (2014) A review of dynamic experimental techniques and mechanical behaviour of rock materials. Rock

Mech Rock Eng 47:1411–1478. https://doi.org/10.1007/s00603-013-0463-y

Zhang ZX, Kou SQ, Jiang LG, Lindqvist PA (2000) Effects of loading rate on rock fracture: fracture characteristics and energy partitioning. Int J Rock Mech Min Sci 37(5):745–762. https://doi.org/10.1016/S1365-1609(00)00008-3

Zhang M, Wu HJ, Li QM, Huang FL (2009) Further investigation on the dynamic compressive strength enhancement of concrete-like materials based on split Hopkinson pressure bar tests, part I:experiments. Int J Impact Eng 36(12):1327–1334. https://doi.org/10.1016/j.ijimpeng.2009.04.009

Zhang N, Ma LJ, Wang MY, Zhang QY, Li J, Fan PX (2017a) Comprehensive risk evaluation of underground energy storage caverns in bedded rock salt. J Loss Prev Process Ind 45:264–276. https://doi.org/10.1016/j.jlp.2016.10.016

Zhang QY, Duan K, Jiao YY, Xiang W (2017b) Physical model test and numerical simulation for the stability analysis of deep gas storage cavern group located in bedded rock salt formation. Int J Rock Mech Min Sci 94:43–54. https://doi.org/10.1016/j.ijrmms.2017.02.015

Zheng ZS (1991) Energy transfer process during rock deformation. Sci China (Ser B) 34(1):104–117

Zhou YX, Xia K, Li XB, Li HB, Ma GW, Zhao J, Zhou ZL, Dai F (2012) Suggested methods for determining the dynamic strength parameters and mode-fracture toughness of rock materials. Int J Rock Mech Min Sci 49:105–112. https://doi.org/10.1016/j.ijrmms.2011.10.004

Zhou N, Han XL, Zhang JX, Li M (2016) Compressive deformation and energy dissipation of crushed coal gangue. Powder Technol 297:220–228. https://doi.org/10.1016/j.powtec.2016.04.026